

# A three-dimensional study of the influence of momentum loss on hydrodynamically unstable premixed flames

Daniel Fernández-Galisteo<sup>a,\*</sup>, Anne Dejoan<sup>a</sup>, Josué Melguizo-Gavilanes<sup>b</sup>,  
Vadim N. Kurdyumov<sup>a</sup>

<sup>a</sup>*Department of Energy, CIEMAT, Avda. Complutense 40, 28040 Madrid, Spain*

<sup>b</sup>*Institut Pprime, UPR 3346, CNRS, ISAE-ENSMA, BP 40109, 86961 Futuroscope-Chasseneuil Cedex, France*

---

## Abstract

The propagation of an isobaric premixed flame into a quiescent gas mixture of fuel and oxidizer contained between two parallel plates is investigated numerically. The plates are separated by a small distance  $h$  and considered as adiabatic. The mixture is assumed to be lean in fuel and the combustion model includes a single-step Arrhenius-type reaction, constant heat capacity and unity fuel Lewis number. Transport properties are considered to be temperature dependent or constant, which allows us to decouple two different instability mechanisms of hydrodynamic nature: (i) Darrieus-Landau (associated with the density change due to thermal expansion) and (ii) Saffman-Taylor (associated with the viscosity contrast). By performing three-dimensional (3D) simulations, the propagation rate and the flame front shape is analyzed as a function of the dimensionless parameter  $a = h/\delta_T$ , where  $\delta_T$  is the thermal thickness of the planar flame. The parameter  $a$  ranges from very small values to large enough ones so that flame curvature between the plates manifests itself. Results show that, as the distance between the plates decreases, loss of momentum enhances the hydrodynamic instability in comparison with that of a freely (unconfined) propagating flame. Likewise, viscosity contrast across the flame brings about an additional destabilizing mechanism. When distance between the plates increases, flame curvature can become important and contribute significantly to the overall propagation rate. Finally, by comparison with the 3D simulations, we show that confinement effects can be effectively described by a two-dimensional formulation written in the limit  $a \rightarrow 0$ , in which momentum conservation is reduced to a linear equation for the velocity similar to Darcy's law.

*Keywords:* Hele-Shaw; confined flow; hydrodynamic instability; premixed flame; single-cusp structure

---

@2022 This manuscript version is made available under the CC-BY-NC-ND 4.0 license: <http://creativecommons.org/licenses/by-nc-nd/4.0/>

## 1. Introduction

The instability produced by the deformation of a planar premixed flame front was first discovered independently by Darrieus (1938) [1] and Landau (1944) [2]. This hydrodynamic instability stems from the deflection of streamlines through the flame front produced by gas expansion, giving rise to a positive growth rate of any small flame wrinkle larger than the characteristic flame thickness in absence of other effects. Insights on stabilizing/destabilizing influence of diffusion processes and gravity on the linear evolution was reported later in further theoretical works [3–6].

The long-term dynamics of hydrodynamically unstable flames makes its study more difficult due to the presence of nonlinearities. In particular, at large times after the initial stages of the linear development of the instability, the flame front reaches a large cellular shape controlled by the geometrical domain size. The nonlinear Michelson-Sivashinsky equation [7] was shown to qualitatively reproduce relevant features of these unstable flames [8–13]. However, its restriction to small thermal expansion has motivated the use of more realistic approaches built on the complete Navier-Stokes equations [14–18]. In agreement with experiments, both theoretical and numerical works show that the nonlinear growth of the Darrieus-Landau instability results in the formation of a monocellular flame with a cusp-like structure (a curved flame with a sharp peak pointing toward the burned gas). In moderate-size domains (of about 40 times the flame thickness), this structure, that fills the entire domain, remains stable. However, for larger domains, secondary structures may appear on the flame. These structures propagate in form of small wrinkles along the flame surface giving the flame evolution an unsteady character. The very recent experiments [12] carried out in a large device (150-cm long  $\times$  50-cm wide) reports a merging/splitting cell process occurring at the long-time evolution of the nonlinear regime. This unsteady process, also reported in numerical studies, has been explained as a result of stochastic influence of background noise [11, 12, 14, 15].

A relevant experimental facility for examining intrinsic flame instabilities is the Hele-Shaw burner. In this device, the flame propagates between two parallel plates separated by a small distance,  $h$ . The plates being made of transparent material makes direct visualization of the flame front possible in a quasi-two-dimensional (quasi-2D) form. To our knowledge, first experimental observations of flame instabilities in Hele-Shaw burners can be traced back to the work of Sharif et al. [19]. Since then, good experimental progress has been made [12, 20–28]. Nevertheless, heat and momentum losses inherent to Hele-Shaw burners may interplay with the intrinsic flame instabilities. This influence was first reported by Joulin and Sivashinsky [29] who performed a linear stability analysis modeling the flame as a thin discontinuity.

The authors concluded that friction-induced pressure gradients, coupled with viscosity contrast, enhance the hydrodynamic instability. The latter viscosity effects are referred to as the Saffman-Taylor instability [30] and is originally associated with the formation of finger-like structures at the interface between two fluids with different viscosity driven by an imposed pressure gradient. If the less viscous fluid displaces the more viscous one, the interface is unstable. The analogy with flames rests upon the viscosity change present between the unburnt and the burnt gas across the front that is also subject to pressure gradients.

The effect of confinement in Hele-Shaw burners have been included in previous numerical works [31–37] through averaged flow properties across  $h$ , thus reducing the problem to a quasi-2D form. This formulation is justified for small gap distances ( $h \rightarrow 0$ ), for which the flame front remains planar between the plates. However, for larger values of  $h$ , flame curvature along the direction perpendicular to the plates may also alter the hydrodynamic instability developing along the transversal direction. In the present paper, the effect of momentum loss on the hydrodynamic instability is investigated via three-dimensional (3D) simulations, in which flame curvature in the direction perpendicular to the plates naturally arises. The dimensionless parameter  $a = h/\delta_T$  (that can be interpreted as a Peclet number), with  $\delta_T$  the thermal thickness of the planar flame, is used as the functional parameter for the study. The 3D analysis includes comparisons with results obtained from quasi-2D simulations performed in the limit  $a \rightarrow 0$  (i.e., the high wall-friction limit), as well as with pure 2D simulations (where the gas friction with the walls is absent). This allows to better assess the importance of momentum loss on the hydrodynamic instability.

## 2. General formulation

A laminar premixed-gas flame propagating in a Hele-Shaw burner is considered. A sketch of this configuration is given in Fig. 1. Note that the study is restricted to a semi-closed system, with the left-end open to the atmosphere and the right-end closed. With this arrangement, the flame propagates into a quiescent gas and flame acceleration is only due to changes in the flame topology, unlike that observed in closed-to-open or open-to-open flame propagation [38–40].

The chemical reaction is modeled by a global irreversible step of the type Fuel + Oxidizer  $\rightarrow$  Products. The corresponding reaction rate (moles of fuel per unit time per unit volume) is given by an Arrhenius law and takes the form  $\omega' = \mathcal{B}\rho'^2 Y_F \exp(-E/\mathcal{R}T')$  for a mixture deficient in fuel, where  $E$  is the overall activation energy,  $T'$  is the temperature,  $\rho'$  is the density,  $Y_F$  is the fuel mass fraction,  $\mathcal{R}$  is the universal gas constant, and  $\mathcal{B}$  is an appropriately defined pre-exponential factor that includes the mass fraction of the oxidant. Primes ( $'$ ) denote dimensional quantities.

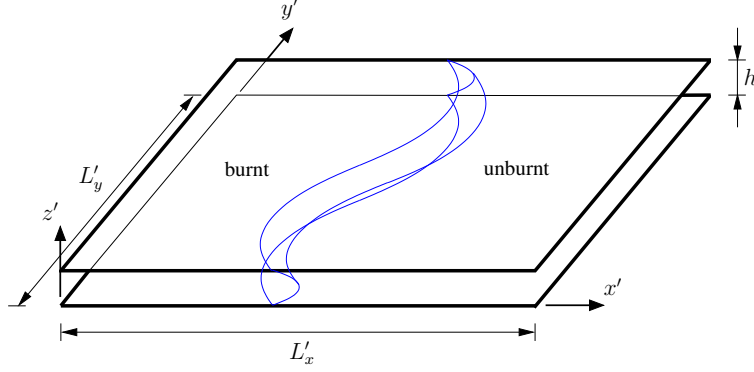


Fig. 1: Schematic view of a curved flame propagating from left to right into a quiescent gas in a Hele-Shaw burner where plates are separated by the distance  $h$ .

The formulation is derived using the low-Mach number approximation and constant mixture heat capacity  $c_p$ , Lewis,  $Le = \mathcal{D}/\mathcal{D}_T$ , and Prandtl,  $Pr = \mu'/(\lambda'/c_p)$ , numbers, where  $\mathcal{D}$  is the mass diffusivity of the fuel;  $\mathcal{D}_T$ ,  $\mu'$  and  $\lambda'$  are the thermal diffusivity, viscosity and thermal conductivity of the gas mixture, respectively. The transport properties are considered to vary with temperature,  $\mu'/\mu_0 = \lambda'/\lambda_0 = (T'/T_0)^\sigma$ , with  $\sigma$  an exponent equals to 0 or 0.7, see [41]. Subscript 0 denotes fresh unburnt mixture.

### 2.1. 3D formulation (finite $h$ )

The full set of the governing equations are scaled using the temperature  $T_0$ , mass fraction  $Y_{F_0}$ , density  $\rho_0$  and viscosity  $\mu_0$  of the unburnt gas. The thermal thickness of the planar flame  $\delta_T = \mathcal{D}_{T_0}/S_L$ , with  $S_L$  the planar burning velocity, is used as the reference length scale, and  $\mathcal{D}_{T_0}/S_L^2$  as the reference time scale. The non-dimensional variables are

$$\begin{aligned} \mathbf{x} &= (x'/\delta_T, y'/\delta_T, z'/\delta_T), \\ \mathbf{u} &= (u'/S_L, v'/S_L, w'/S_L), \\ t &= t' S_L^2 / \mathcal{D}_{T_0}, \quad \rho = \rho' / \rho_0, \quad p = (p' - p_{\text{atm}}) / \rho_0 S_L^2, \\ \theta &= (T' - T_0) / (T_a - T_0), \quad Y = Y_F / Y_{F_0}, \end{aligned}$$

where  $T_a = T_0 + QY_{F_0}/c_p$  is the adiabatic temperature, with  $Q$  the heat of combustion. The dimensionless equations, written in a reference frame moving at flame front velocity  $u_f$  with respect to the wall, read

$$\frac{\partial \rho}{\partial t} + \nabla \cdot [\rho(\mathbf{u} - u_f)] = 0, \quad (1)$$

$$\begin{aligned} \frac{\partial(\rho \mathbf{u})}{\partial t} + \nabla \cdot [\rho \mathbf{u}(\mathbf{u} - u_f)] &= -\nabla p + \\ Pr \nabla \cdot [\mu(\nabla \mathbf{u} + \nabla \mathbf{u}^T) - 2/3 \mu(\nabla \cdot \mathbf{u}) \mathbf{I}], \end{aligned} \quad (2)$$

$$\frac{\partial(\rho \theta)}{\partial t} + \nabla \cdot [\rho \theta(\mathbf{u} - u_f)] = \nabla \cdot (\mu \nabla \theta) + \omega, \quad (3)$$

$$\frac{\partial(\rho Y)}{\partial t} + \nabla \cdot [\rho Y(\mathbf{u} - u_f)] = \frac{1}{Le} \nabla \cdot (\mu \nabla Y) - \omega, \quad (4)$$

with the ideal gas equation of state

$$\rho(1 + q\theta) = 1, \quad (5)$$

and the reaction rate given by

$$\omega = \frac{\beta^2}{2u_p^2 Le} (1+q)^{2-\sigma} \rho^2 Y \exp\left\{ \frac{\beta(\theta-1)}{(1+q\theta)/(1+q)} \right\}. \quad (6)$$

The remaining parameters are: the Zel'dovich number  $\beta = E(T_a - T_0)/\mathcal{R}T_a^2$ , the thermal expansion coefficient  $q = (T_a - T_0)/T_0$ , and the exponent  $\sigma$  of the viscosity law  $\mu = (1+q\theta)^\sigma$ . In this work we assume  $\beta = 10$ ,  $q = 5$ ,  $Le = 1$ , and  $Pr = 0.7$ , as representative of hydrocarbon combustion;  $\sigma = 0$  or  $\sigma = 0.7$  for constant or temperature dependent viscosity, respectively.

The factor  $u_p = S_L/U_L$  in (6) is introduced to account for the difference between the asymptotic ( $\beta \gg 1$ ) value of the planar burning velocity,  $U_L$ , and the value of  $S_L$  for finite  $\beta$ , and ensures that the velocity of the planar flame equals one in the computations. The values of  $u_p$  are 1.0547 for  $\sigma = 0$  and 0.9997 for  $\sigma = 0.7$  (see [33] for further details).

The normalized flame velocity  $u_f$  is determined by

$$u_f = \frac{1}{aL_y} \int_0^{L_x} \int_0^{L_y} \int_0^a \omega \, dx \, dy \, dz. \quad (7)$$

The term  $u_f$  is also known as the overall propagation rate,  $S_c/S_L$ , with  $S_c$  the consumption speed.

The mathematical problem described in Eqs. (1)-(6) is solved with the general boundary conditions

$$z = 0, a: \quad \mathbf{u} = \partial\theta/\partial z = \partial Y/\partial z = 0, \quad (8)$$

$$x \rightarrow -\infty: \quad \partial \mathbf{u} / \partial x = \partial \theta / \partial x = \partial Y / \partial x = 0, \quad (9)$$

$$x \rightarrow +\infty: \quad \mathbf{u} = \theta = Y - 1 = 0, \quad (10)$$

and periodic conditions in the  $y$ -direction.

The initial condition is a planar flame to which a weak harmonic perturbation in the form  $\epsilon \cos(ky) \exp(-|x - x_\omega|)$  is added in the temperature field. The amplitude of the perturbation  $\epsilon$  is set to  $10^{-2}$ , with  $x_\omega$  the position of the maximum reaction rate and  $k$  the wavenumber. In all simulations presented below, the wavenumber of the perturbation,  $k = 2\pi n/L_y$ , is fixed to the maximum growth rate obtained from the linear stability analysis [35] in the limit  $a = h/\delta_T \rightarrow 0$ . Here,  $n$  corresponds to the number of waves set for the initial perturbation.

## 2.2. Quasi-2D formulation ( $h \ll \delta_T$ )

In the limit  $a = h/\delta_T \rightarrow 0$ , the governing equations (1)-(4) can be reduced to a 2D set of equations, referred to as the quasi-2D form hereafter. Indeed, averaging flow quantities across the gap distance  $h$  reduces the momentum equation (2) to a linear relation for the velocity similar to Darcy's law

$$\mathbf{u} = -\frac{1}{12\mu Pr} \nabla p, \quad (11)$$

where the operator  $\nabla$  is defined in the  $xy$ -plane only. The derivation of the quasi-2D formulation is out of the scope of this paper; the reader is referred to [33, 34] for further details. This formulation results in a drastic reduction of the computational cost compared with the full 3D description. Although the limit  $a \rightarrow 0$  has shown reasonable agreement with experimental observations [33], its range of validity has not been tested explicitly.

## 2.3. Pure 2D formulation (unconfined geometry)

This case corresponds to the classical 2D formulation where the vector operators in Eqs. (1)-(4) are defined in the  $xy$ -plane only. Pure 2D simulations have been used extensively in the context of hydrodynamic (and diffusive-thermal) theory [14–18].

## 3. Numerical treatment

Transient computations are carried out in a finite domain of dimensions  $L_x \times L_y \times a$  in the respective longitudinal, transversal and normal directions. The set of Eq. (1)-(4) are integrated using the Open source Field Operation And Manipulation (OpenFOAM) toolbox [42]. The code is based on the finite volume method formulated in a collocated grid arrangement. The pressure-velocity coupling to ensure mass conservation is realized making use of the PIMPLE iterative algorithm. A first-order Euler scheme is used for temporal discretization whereas for spatial discretization a second-order scheme is used.

A grid resolution of  $\Delta_x = \Delta_y = \Delta_z = 0.1$  was shown to be sufficient to correctly capture the flame evolution. Doubling the resolution did not result in appreciable changes in the flame dynamics. For the smallest values of  $a$  employed in this work, the resolution in the normal direction was reduced to  $\Delta_z = 0.006$  to capture the development of the Poiseuille flow profile. Finally,  $L_x$  is taken to be twice  $L_y$  to avoid any influence of boundary conditions on the solution, and a fixed time step equal to  $\Delta_t = 5 \times 10^{-5}$  is used for numerical stability. The total computational cost of the study is approximately  $1.25 \times 10^6$  CPU hours.

## 4. Length scale considerations

The temperature dependence of viscosity modifies the flame thickness compared to that obtained

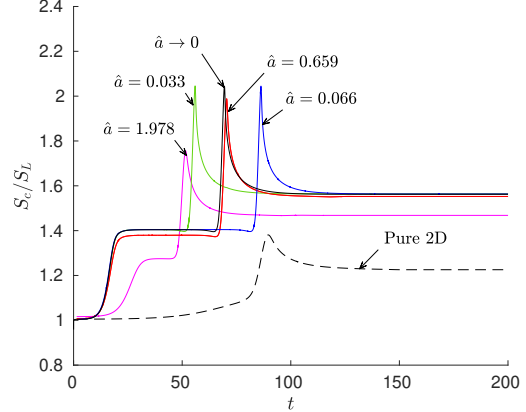


Fig. 2: The variation of the propagation rate with time for constant viscosity ( $\sigma = 0$ ) and  $\hat{a} = 0$  (quasi-2D), 0.033, 0.066, 0.659, and 1.978. Transversal size is  $\hat{L}_y = 26.3$ . Pure 2D simulation is plotted with dashed curve.

assuming constant viscosity [31]. The length scale  $\delta_T$  used to normalize Eqs. (1)-(6) does not maintain identical domain size to flame thickness ratio between the variable and the constant viscosity cases. A more appropriate length scale that enables us to make better comparisons is the flame thickness based on the maximum temperature gradient  $\delta_f = (T_a - T_0) / \max(dT/dx')$ . For a meaningful comparison between constant and variable viscosity cases,  $\delta_f$  is thus used to re-scale the size of the computational domain. Based on planar flame computations, the ratio  $\delta_f/\delta_T$  is 1.52 and 4.34 for  $\sigma = 0$  and 0.7, respectively. This implies that the domain employed for  $\sigma = 0$  must be re-scaled by a factor of 2.86 when computing cases using  $\sigma = 0.7$ . To simplify the discussion below, the hat symbol is used to refer to variables normalized with  $\delta_f$ , i.e.  $\hat{\mathbf{x}} = \mathbf{x}/\delta_f$ ,  $\hat{a} = h/\delta_f$ , and  $\hat{L}_y = L_y/(\delta_f/\delta_T)$ .

## 5. Results and discussion

The influence of momentum loss and viscosity contrast is first analyzed in Section 5.1 by varying  $\hat{a}$  and keeping  $\hat{L}_y$  fixed. In Section 5.2, the influence of  $\hat{L}_y$  is analyzed. The effect of flame curvature along the  $z$ -direction is investigated in Section 5.3. A brief summary is finally given in Section 5.4.

### 5.1. Momentum loss and viscosity contrast effects

Figure 2 compares the time evolution of the overall propagation rate,  $S_c/S_L$ , for  $\hat{a} \rightarrow 0$  (quasi-2D) and finite values of  $\hat{a}$  ranging from 0.033 to 1.978, with results obtained from the pure 2D formulation. The size of the transversal domain is fixed to  $\hat{L}_y = 26.3$ , for which the maximum growth rate of the perturbation is set using  $n = 2$ . As a result, the initially planar flame destabilizes into two cusps to finally reach,

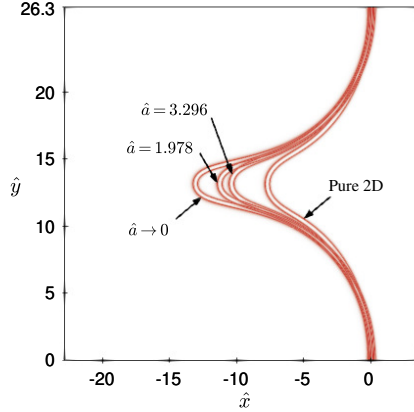


Fig. 3: Illustration of the single-cusp structure represented by the reaction rate isocontour ( $\omega = 1$ ) in the plane  $\hat{z} = 0$  for different values of  $\hat{a}$  and for the pure 2D simulation. Same conditions as given in Fig. 2.

at large times, a single cusp that fills the entire domain and remains steady (see the flame structure in Fig. 3). The peaks in the  $S_c/S_L$  curve are associated with merging of the two cusps. For  $\hat{a} \leq 0.659$  all cases converge to the final value of  $S_c/S_L \approx 1.56$ , but for  $\hat{a} = 1.978$  the propagation rate decreases by 5%. The figure clearly shows that the propagation rate is larger in the presence of confinement than in the case where the geometry is unconfined (pure 2D simulation).

Figure 3 illustrates the flame front topology (represented by the reaction rate isocontour  $\omega = 1$ ) for different values of  $\hat{a}$  and for the conditions given in Fig. 2. The flame propagates from left to right. As expected, the increase in the propagation rate is due to the increase in the flame surface area. Because of the gas friction with the walls, the motion of the hot-gas products in the left side induces a higher strain near the trough (the region that is concave toward the fresh mixture) as  $h$  decreases, significantly elongating the flame surface. By reference to the pure 2D simulation, in which the flame cusp manifests only through thermal expansion, Figs. 2 and 3 indicate that momentum loss (related to confinements effects) enhances the instability mechanism associated to thermal expansion, and that the 3D simulations are in close agreement with the quasi-2D formulation for  $\hat{a} \lesssim 1$ . For larger  $\hat{a}$ , contribution of wall friction to longitudinal pressure gradient decreases, which in turn, reduces the flame elongation and thus flame propagation speed. Note that as  $\hat{a}$  increases flame curvature may also occur in the direction perpendicular to the plates (along  $z$ ); see Section 5.3.

The time evolution of the propagation rate for variable viscosity ( $\sigma = 0.7$ ) is shown in Fig. 4. Similarities with the dynamics described in Fig. 2 for  $\hat{a} \geq 0.659$  are evident. However, for  $\hat{a} \leq 0.066$ , spo-

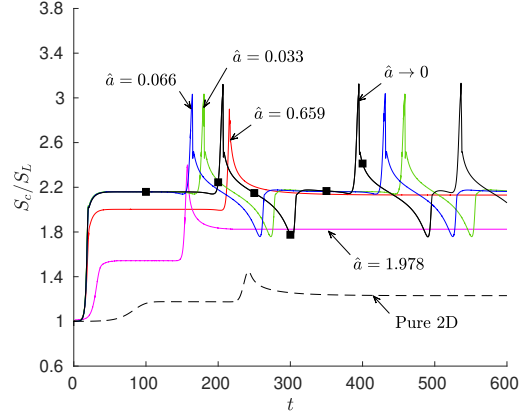


Fig. 4: The variation of the propagation rate with time for variable viscosity ( $\sigma = 0.7$ ) and  $\hat{a} = 0, 0.033, 0.066, 0.659$ , and  $1.978$ . Transversal size is  $\hat{L}_y = 26.3$ . Pure 2D simulation is plotted with dashed curve.

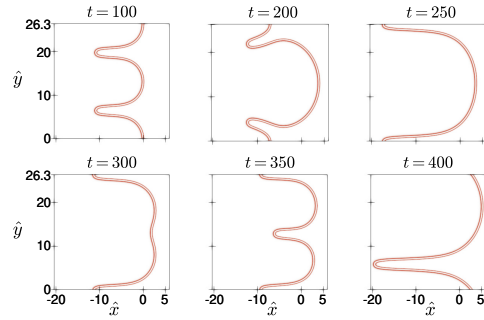


Fig. 5: Evolution of the flame front topology represented by the reaction rate isocontour ( $\omega = 0.2$ ). The snapshots are taken at the times marked with square symbols in Fig. 4 for  $\hat{a} \rightarrow 0$ .

radic oscillations are obtained. An increase in spatial resolution (up to a factor 10) did not affect/suppress the oscillatory temporal behavior, as it results from the merging/splitting of the flame cusps. To illustrate this process, the flame front evolution for  $\hat{a} \rightarrow 0$  is plotted in Fig. 5 at representative times (marked with square symbols in Fig. 4). The initial two cusps ( $t = 100$ ) destabilize at  $t = 200$  to merge into one cusp at  $t = 250$ . Subsequently, this one-cusp flame front splits again into two cusps (between  $t = 300$  and  $t = 350$ ) to finally recover a one-cusp shape ( $t = 400$ ). Note that the single-cusp structure shown at  $t = 250$  and  $t = 400$  are similar, the only difference being the displacement in the transversal position; the local minima in the  $S_c/S_L$  curve are associated with splitting of the crest (the leading part of the flame) while peaks are associated with merging of the cusps. The merging/splitting process repeats over time and it is similar to that previously observed in pure 2D studies [11–16] and experiments [12] in large

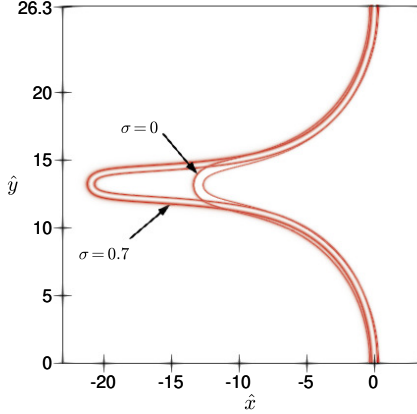


Fig. 6: Illustration of the single-cusp structure represented by the reaction rate isocontour ( $\omega = 0.2$ ) in the plane  $\hat{z} = 0$  for constant viscosity ( $\sigma = 0$ ) and variable viscosity ( $\sigma = 0.7$ ). Calculated for  $\hat{L}_y = 26.3$  and  $\hat{a} = 0.659$ .

domains. The appearance of this unsteady dynamics depends on  $\hat{L}_y$  and it is briefly analyzed in the next section.

The main consequence of introducing variable viscosity is an increase in the overall propagation rate. This increase is significant for small  $\hat{a}$ . For instance, for  $\hat{a} = 0.659$ , variable viscosity increases  $S_c/S_L$  by about a 35% relative to the constant viscosity case. The comparison of the corresponding topologies is illustrated in Fig. 6. The flame surface is further elongated when variable viscosity is considered, indicating that viscosity contrast may induce an additional destabilizing mechanism. In absence of confinement, however, viscosity contrast plays a minor role. This is clearly seen when comparing the pure 2D simulation in Figs. 2 and 4. In both cases,  $S_c/S_L \approx 1.23$  at the final evolution.

### 5.2. Transversal domain size variation

The oscillations observed in Fig. 4, associated with the transversal domain size, have been discussed extensively in the context of pure 2D simulations. Our interest here is on determining the onset of unsteadiness when momentum loss is present. Figure 7 shows  $S_c/S_L$  at the final evolution as a function of  $\hat{L}_y$  for both constant and variable viscosity. Due to the high computational cost, only quasi-2D and pure 2D simulations are compared. As expected, the propagation rate corresponds with the planar velocity ( $S_c/S_L = 1$ ) when the transversal size is below a critical value,  $\hat{L}_{y,c}$ . Above this critical length, the flame destabilizes into a single cusp and the propagation rate increases steadily with  $\hat{L}_y$  until it reaches a plateau. For large  $\hat{L}_y$ , the unsteady oscillatory behaviour described in the previous section emerges. This latter is indicated with empty circles in Fig. 7, for which the propagation

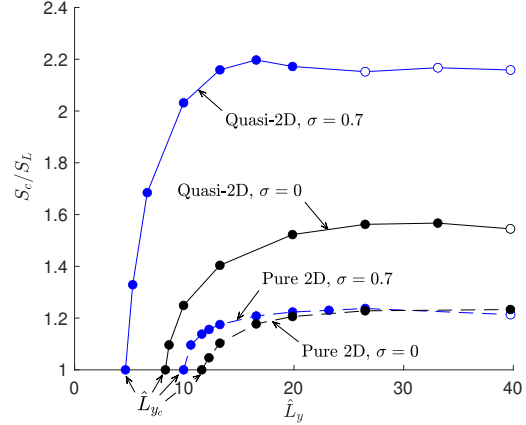


Fig. 7: The variation of the propagation rate with transversal size domain  $\hat{L}_y$  for constant ( $\sigma = 0$ ) and variable ( $\sigma = 0.7$ ) viscosity, given for quasi-2D (high confinement) and 2D (no confinement) geometries. Empty circles stand for unsteady flame regime.

rate is calculated as a time-averaged value. As can be seen, variable viscosity and/or confinement trigger the onset of oscillations at smaller  $\hat{L}_y$  than constant viscosity and/or unconfined geometries. The figure shows that the quantitative effect of wall-friction and viscosity contrast (in terms of the propagation velocity) is domain-size dependent.

There is agreement between the value of  $\hat{L}_{y,c}$  found in our simulations with those reported in linear stability studies. For instance, the value of  $\hat{L}_{y,c} = 11.7$  for the pure 2D simulation ( $\sigma = 0$ ) agrees well with the value reported by Sharpe et al. [18]; and the value of  $\hat{L}_{y,c} = 8.3$  for the quasi-2D simulation ( $\sigma = 0$ ) coincides with that reported in [35]. The upper limit of the propagation velocity for the pure 2D problem is also in agreement with previous studies in the context of the nonlinear development of hydrodynamic flames [15–17, 43, 44]. For instance, Bychkov et al. [43] reported a value of  $S_c/S_L \approx 1.22$ , and Al-tantzis et al. [16] reported a value of  $S_c/S_L \approx 1.25$ , both in agreement with that found in the present study ( $S_c/S_L \approx 1.23$ ).

### 5.3. Curvature along the gap distance

The hydrodynamic mechanism at the origin of the cusp-like structure in the  $xy$ -plane can also alter the flame shape in the  $xz$ -plane. Obviously, because of the different boundary conditions in the transversal  $xy$ -plane (periodic) and in the normal  $xz$ -plane (non-slip), the hydrodynamic effect manifests itself differently on the flame topology in each plane.

Figure 8 illustrates the flame topology that emerges in the  $xz$ -plane for  $\sigma = 0.7$  and for increasing values of  $\hat{a}$ . Of interest here is the existence of a critical gap distance,  $\hat{a}_c$ , above which the symmetric flame desta-

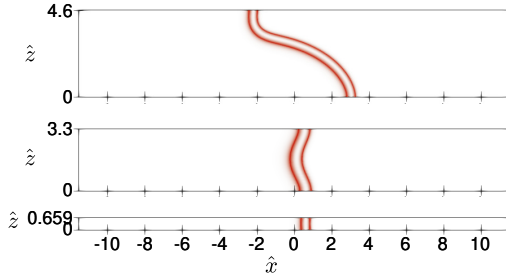


Fig. 8: Illustration of the flame curvature along  $h$  represented by the reaction rate isocontour ( $\omega = 0.2$ ) in the plane  $\hat{y} = 0$ , for  $\sigma = 0.7$  and  $\hat{a} = 0.659, 3.3$ , and  $4.6$ .

bilizes into a non-symmetric shape, as shown in Fig. 8 (top). According to [45], when the non-symmetric flame solution exists, it is stable and the corresponding symmetric solution is unstable; the unstable symmetric solution can be forced by halving the computational domain in the  $h$  direction (i.e.  $L_x \times L_y \times h/2$ ) and imposing a symmetry boundary condition on the  $z = h/2$ -plane. Expectedly, non-symmetric shapes result in a significant increase of the flame surface area and consequently in the propagation velocity. This is illustrated in Fig. 9, where the variation of the propagation rate with  $\hat{a}$  is shown for  $\hat{L}_y = 13.15$ . In this figure, triangles correspond to non-symmetric flame solutions whereas filled and empty circles represent stable and unstable (forced) symmetric solutions, respectively. The critical gap distance is in accordance with the value  $\hat{a}_c \approx 3.9$  reported for a planar channel in [45, 46].

Figure 10 shows the 3D flame shapes obtained for the non-symmetric (top) and the forced symmetric (bottom) solutions, for  $\hat{a} = 4.6$  and  $\hat{L}_y = 13.15$ . Note the significantly reduced (or even suppressed) elongation of the cusp in the  $xy$ -plane for the non-symmetric flame compared to the symmetric flame. Clearly, the high curvature of the non-symmetric flame along the  $xz$ -plane may play some role. This outcome suggests that flame curvature in the gap distance competes with that present in the  $xy$ -plane. In the case of Fig. 10 (top), the main contribution to the propagation rate reported in Fig. 9 comes from the flame curvature along  $xz$ -plane. A well formed flame cusp in the  $xy$ -plane would certainly occur by further increasing  $\hat{L}_y$ , but was not considered here due to the high computational cost.

#### 5.4. Summary

Figure 9 summarizes nicely our results. For small  $\hat{a}$  the difference in the propagation velocity between variable and constant viscosity is appreciable. The propagation velocity and the difference between  $\sigma = 0$  and  $\sigma = 0.7$  diminishes as the gap distance increases, approaching the pure 2D formulation results;

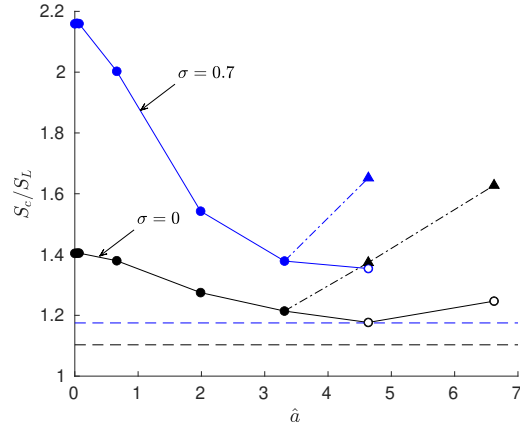


Fig. 9: The variation of the propagation rate with gap distance  $\hat{a}$ , calculated for  $\hat{L}_y = 13.15$ . Filled and empty circles stand for stable and unstable (forced) symmetric flame solutions in the  $xz$ -plane. Triangles indicate stable non-symmetric solutions. Dashed lines represent pure 2D formulation values.

confinement effects may thus be considered negligible. However, for  $\hat{a} \geq 4$ , the propagation velocities (denoted with a dashed-dotted line) increase again due to the high flame curvature in the  $xz$ -plane that results from a non-symmetric shape. Finally, note that Fig. 9 was obtained for  $\hat{L}_y = 13.15$ , a transversal size for which all flames have a final steady solution.

## 6. Conclusions

Confinement effects on the large-scale hydrodynamic instability of a flame propagating between two adiabatic plates was analyzed in three dimensions by varying the distance separating the plates,  $h$ . The limit  $a = h/\delta_T \rightarrow 0$  (high friction limit) and the pure 2D simulations (no confinement) were also considered and used for comparisons. The present numerical study confirms the analytical results anticipated by Joulin and Sivashinsky [29] in the linear regime: i) high wall friction and ii) viscosity contrast reinforce the hydrodynamic instability. Our results also show that there is a critical distance ( $h/\delta_f \approx 3.9$ ) above which flame curvature in the  $xz$ -plane (that of a non-symmetric shape) can compete with the large-scale single cusp that develops in the  $xy$ -plane, resulting in stabilizing effects. The emergence of an unsteady regime, associated with a successive merging/splitting process of the cusps, as previously discussed in the literature, is also reported in the present study. However, it is found that the unsteady behavior is triggered for a smaller size  $\hat{L}_y$  of the domain in presence of high confinement and/or variable viscosity. Finally, the quasi-2D formulation was found to provide very satisfactory results up to  $a \approx 1$ , when comparing to the 3D simulations.



- [25] F. Veiga-López, D. Martínez-Ruiz, M. Kuznetsov, M. Sánchez-Sanz, Thermoacoustic analysis of lean premixed hydrogen flames in narrow vertical channels, *Fuel* 278 (2020) 118212.
- [26] F. Veiga-López, M. Kuznetsov, D. Martínez-Ruiz, E. Fernández-Tarrazo, J. Grune, M. Sánchez-Sanz, Unexpected propagation of ultra-lean hydrogen flames in narrow gaps, *Phys. Rev. Lett.* 124 (2020) 174501.
- [27] M. Tayyab, B. Radisson, C. Almarcha, B. Denet, P. Boivin, Experimental and numerical Lattice-Boltzmann investigation of the Darrieus-Landau instability, *Combust. Flame* 221 (2020) 103–109.
- [28] G. Gu, J. Huang, W. Han, C. Wang, Propagation of hydrogen-oxygen flames in Hele-Shaw cells, *Int. J. Hydrogen Energy* 46 (2021) 12009–12015.
- [29] G. Joulin, G. I. Sivashinsky, Influence of momentum and heat losses on the large-scale stability of quasi-2D premixed flames, *Combust. Sci. Technol.* 98 (1994) 11–23.
- [30] P. G. Saffman, S. G. Taylor, The penetration of a fluid into a porous medium or Hele-Shaw cell containing a more viscous liquid, *Proc. Roy. Soc. London, A* 245 (1958) 312–329.
- [31] S. H. Kang, H. G. Im, S. W. Baek, A computational study of Saffman-Taylor instability in premixed flames, *Combust. Theory Model.* 7 (2003) 343–363.
- [32] S. H. Kang, S. W. Baek, H. G. Im, Effects of heat and momentum losses on the stability of premixed flames in a narrow channel, *Combust. Theory Model.* 10 (4) (2006) 659–681.
- [33] D. Fernández-Galisteo, V. N. Kurdyumov, P. D. Ronney, Analysis of premixed flame propagation between two closely-spaced parallel plates, *Combust. Flame* 190 (2018) 133–145.
- [34] D. Martínez-Ruiz, F. Veiga-López, D. Fernández-Galisteo, V. N. Kurdyumov, M. Sánchez-Sanz, The role of conductive heat losses on the formation of isolated flame cells in Hele-Shaw chambers, *Combust. Flame* 209 (2019) 187–199.
- [35] D. Fernández-Galisteo, V. N. Kurdyumov, Impact of the gravity field on stability of premixed flames propagating between two closely spaced parallel plates, *Proc. Combust. Inst.* 37 (2019) 1937–1943.
- [36] T. Miroshnichenko, V. Gubernov, S. Minaev, Hydrodynamic instability of premixed flame propagating in narrow planar channel in the presence of gas flow, *Combust. Theory Model.* 24 (2020) 362–375.
- [37] Y. Han, M. Modestov, D. M. Valiev, Effect of momentum and heat losses on the hydrodynamic instability of a premixed equidiffusive flame in a Hele-Shaw cell, *Phys. Fluids* 33 (2021) 103608.
- [38] V. Bychkov, A. Petchenko, V. Akkerman, L. E. Eriksson, Theory and modeling of accelerating flames in tubes, *Phys. Rev. E* 72 (2005) 046307.
- [39] V. Akkerman, C. K. Law, V. Bychkov, L. E. Eriksson, Analysis of flame acceleration induced by wall friction in open tubes, *Phys. Fluids* 22 (2010) 053606.
- [40] V. N. Kurdyumov, M. Matalon, Self-accelerating flames in long narrow open channels, *Proc. Combust. Inst.* 35 (2015) 921–928.
- [41] M. D. Smooke, V. Giovangigli, Formulation of the premixed and non-premixed test problems, in: M. D. Smooke (Ed.), *Reduced Kinetic Mechanisms and Asymptotic Approximations for Methane-Air Flames*, Vol. 384 of *Lecture Notes in Physics*, Springer-Verlag, 1991, pp. 1–28.
- [42] H. G. Weller, G. Tabor, H. Jasak, C. Fureby, A tenorial approach to computational continuum mechanics using object-oriented techniques, *Comput. Phys.* 12 (1998) 620–631.
- [43] V. V. Bychkov, S. M. Golberg, M. A. Liberman, L. E. Eriksson, Propagation of curved stationary flames in tubes, *Phys. Rev. E* 54 (1997) 3713.
- [44] V. V. Bychkov, Nonlinear equation for a curved stationary flame and the flame velocity, *Phys. Fluids* 10 (1998) 2091–2098.
- [45] A. Dejoan, C. Jiménez, V. N. Kurdyumov, Critical conditions for non-symmetric flame propagation in narrow channels: Influence of the flow rate, the thermal expansion, the Lewis number and heat-losses, *Combust. Flame* 209 (2019) 430–440.
- [46] C. Jiménez, D. Fernández-Galisteo, V. N. Kurdyumov, Flame-acoustics interaction for symmetric and non-symmetric flames propagating in a narrow duct from an open to a closed end, *Combust. Flame* 225 (2021) 499–512.